International Journal of Solids and Structures xxx (xxxx) xxx

Contents lists available at ScienceDirect

International Journal of Solids and Structures

journal homepage: www.elsevier.com/locate/ijsolstr

Vibration isolation of few-layer graphene sheets

Lu Lu[a,b], C.Q. Ru[b], Xingming Guo[a,*]

[a] Shanghai Institute of Applied Mathematics and Mechanics, Shanghai Key Laboratory of Mechanics in Energy Engineering, Shanghai University, Shanghai 200072, People's Republic of China
[b] Department of Mechanical Engineering, University of Alberta, Edmonton T6G 2G8, Canada

ARTICLE INFO

Article history:
Received 17 July 2018
Revised 28 February 2019
Accepted 21 August 2019
Available online xxx

Keywords:
Few-layer graphene
Multi-layer graphene
Metamaterial
Negative mass
Bandgap
Vibration isolation

ABSTRACT

This work shows that a few-layer graphene with two highly-tensioned outermost layers exhibits negative effective mass and behaves like an elastic metamaterial. Actually, our simulations based on simple elastic membrane model confirm the existence of a bandgap in terahertz range within which a tensioned few-layer graphene exhibits remarkable vibration isolation: forced vibration will be highly restricted to a narrow region around the site of the applied excitation while all other parts of the graphene remain essentially static. The values of terahertz bandgap frequencies are determined by the van der Waals interaction coefficient between adjacent layers, while the width of the bandgap is determined by the number of inner layers. This research may provide new perspectives for designing and analyzing graphene-based metamaterials and nano-resonators with potential applications in high-frequency vibration controlling.

1. Introduction

Acoustic/elastic metamaterials are artificial materials characterized by negative effective mass and/or negative effective modulus, which have received great attention in last two decades due to their unusual dynamic properties in manipulating elastic waves and vibration (Lee and Wright, 2016; Ma and Sheng, 2016). Acoustic/elastic metamaterials exhibiting negative effective properties are commonly attributed to frequency bandgap generated by local resonance of artificially designed structural units, within which elastic vibration and waves are largely suppressed (Liu et al., 2000, 2005; Milton and Willis, 2007; Yao et al., 2008; Huang et al., 2009). Based on this concept, various acoustic/elastic metamaterials with negative effective properties have been proposed, with potential application to such as vibration isolation, wave attenuation and energy harvesting (Wang, 2014; Li and Wang, 2016; Oudich and Li, 2017; Jiang and He, 2017; Oh et al., 2017; Chen et al., 2017; Beli et al., 2018; Chang et al., 2018). To mention a few, Yang et al. (2008) fabricated a membrane-type metamaterial which demonstrates negative dynamic mass within the frequency range 200–300 Hz, with the basic unit composed of a circular elastic membrane with a small weight attached to the center. Zhu et al. (2014) designed a chiral-lattice-based elastic metamaterial beam with multiple embedded resonators to realize broadband vibration suppression. Li et al. (2017) attached a square array of free-standing cantilevers to a primary structural frame to achieve a metamaterial for simultaneous vibration isolation and energy harvesting. By using a generalized Maxwell model, Lewinska et al. (2017) investigated the attenuation performance of a locally resonant acoustic metamaterial consisting of multi-coated coaxial inclusions of rubber and tungsten embedded in epoxy. Clearly, one real challenge in the design of acoustic/elastic metamaterial is how to achieve the often complicated artificial microstructure at small scales for the desirable negative effective properties and dynamic behaviors.

In spite of numerous works on artificially designed elastic metamaterials, graphene-based elastic metamaterials with negative effective mass remain unexplored. Graphene, as a single atom thick two-dimensional carbon material, possesses many extraordinary mechanical and electronic properties (Lee et al., 2008; Castro Neto et al., 2009), and holds great potential in nanotechnology. In particular, mechanical vibration of few- or multi-layer graphene sheets has been an active topic of current interest and been extensively studied experimentally or theoretically in the past 15 years (Bunch et al., 2007; Frank et al., 2007; Castellanos-Gomez et al., 2015; Khan et al., 2017). For instance, Garcia-Sanchez et al. (2008) detected mechanical vibration and measured resonance frequencies of a multi-layer graphene-based nanoelectromechanical systems using scanning probe microscopy. With the help of an atomic force microscope, Poot and van der Zant (2008) measured the mechanical properties of suspended few-layer graphene membranes and estimated their fundamental resonance frequencies. More recently, because multi-layer graphene sheets grown by available techniques

* Corresponding author.
E-mail address: xmguo@shu.edu.cn (X. Guo).

https://doi.org/10.1016/j.ijsolstr.2019.08.029
0020-7683/

are usually incommensurate with vanishingly low interlayer in-plane coupling (Dienwiebel et al., 2004; Xu et al., 2012; Koshino, 2015; Han et al., 2016), the present authors (Lu et al., 2017) developed a simplified 3-beam model to study mechanical vibration of multi-layer graphene sheets whose two outermost layers are highly tensioned while all inner layers are tension-free or less-tensioned. However, all of the aforementioned works are limited to classical vibrational behavior of few- or multi-layer graphene sheets and have not revealed any metamaterial-like vibrational behavior such as vibration isolation.

Motivated by an idea that the interlayer degrees of freedom of a multi-layer graphene sheet could offer a locally-resonant microstructure, the present work aims to study metamaterial-like vibrational behavior of multi-layer graphene sheets. Here, for simplicity, we shall focus on few-layer graphene sheets (of typically, say 3–6 layers) already fabricated in recent literature (Hao et al., 2010; Lui et al., 2012; Kumar et al., 2013) whose two outermost layers are highly tensioned while all inner layers are tension-free or less-tensioned. The present paper shows that few-layer graphene sheets with highly tensioned two outermost layers exhibit remarkable metamaterial-like elastic dynamic behavior within a certain frequency range. In particular, it will be shown that the order of magnitude of bandgap frequencies of a FLGS is determined by the van der Walls interaction coefficient between adjacent layers, and the width of the bandgap is determined by the number of inner layers. Here it should be mentioned that in terahertz physics, forced vibration or wave propagation of nanoscale device or structures can be stimulated by external periodic stimulus at terahertz frequencies which are much higher than their own natural frequencies, such as plasma oscillation (Wang et al., 2014), optical pulse (Jnawali et al., 2013), infrared (Ren et al., 2012) and radiation (Svintsov et al., 2014). Therefore, it is of potential interest to investigate terahertz forced vibration of graphene-based nanoscale devices and structures even when their own natural frequencies are much below terahertz.

2. Elastic membrane model for few-layer graphene sheets

The present work studies metamaterial-like vibration of multi-layer graphene sheet (MLGS) with two highly-tensioned outmost layers and tension-free or less-tensioned inner layers which offer a possible locally-resonant microstructure. Since MLGSs grown by available techniques are usually incommensurate with ultralow interlayer friction (typically, the interlayer friction coefficient for incommensurate multi-layer graphene is on the order of 0.001) (Dienwiebel et al., 2004; Xu et al., 2012; Koshino, 2015; Han et al., 2016), tension forces applied directly to two outermost layers of a MLGS could not be transferred into all inner layers. For this reason, it is practically realistic to assume that all inner layers of a tensioned MLGS are much less-tensioned or nearly tension-free. Therefore, in this work, we shall consider a tensioned few-layer graphene sheet (FLGS) of length L whose two outermost layers are highly tensioned while all inner layers are tension-free or less-tensioned, as shown in Fig. 1. Throughout the paper, it is assumed that the two outermost (top and bottom) singlelayers are highly tensioned under the same tension force T (per unit width), and each of all inner singlelayers is tension-free or subjected to a lower tension force δ_T ($0 \le \delta \le 1$). Because the bending rigidity of a singlelayer or few-layer graphene sheet is usually neglected when it is highly tensioned by a significant tension force (say, >0.1 N/m) (Bunch et al., 2007; Frank et al., 2007; Garcia-Sanchez et al., 2008; Castellanos-Gomez et al., 2015), the bending rigidity of the FLGS is neglected in the present paper. In other words, each of all singlelayer graphene sheets of the FLGS is treated as an elastic membrane with zero bending rigidity.

To study flexure vibration of a tensioned FLGS, the FLGS is modeled as a simplified 3-membrane system (Lu et al., 2017), as shown in Fig. 1, in which the two outermost (top and bottom) layers are modeled as two membranes, and all inner layers (which are all tension-free or equally tensioned by a lower tension force δ_T, $0 \le \delta \le 1$) together are modeled as another single membrane. The three membranes are coupled through van der Waals interaction between any two adjacent membranes. Here it should be stated that the 1D elastic membrane models have been widely used in various related papers on vibration of graphene sheets, see Atalaya et al., 2008; Chen et al. (2009), van der Zande et al. (2010). Thus, for flexural vibration of the FLGS characterized by the in-phase condition $w_1 = w_3$ of the top and bottom layers, the governing equations of the FLGS can be written as (see Eq. (8) of Lu et al. (2017))

$$\begin{cases} -T\frac{\partial^2 w_1}{\partial x^2} + \rho h\frac{\partial^2 w_1}{\partial t^2} = c(w_2 - w_1) \\ -\delta m T\frac{\partial^2 w_2}{\partial x^2} + m\rho h\frac{\partial^2 w_2}{\partial t^2} = 2c(w_1 - w_2) \end{cases} \tag{1}$$

where w_1 and w_2 are the transverse deflection of the top (bottom) layer and the inner layers, respectively, t is time, $\rho = 2200\,\mathrm{kg/m^3}$ is the mass density of graphene, m is the number of inner layers, $h = 0.34\,\mathrm{nm}$ is the (nominal) thickness of singlelayer graphene, and $c = 99\,\mathrm{GPa/nm}$ is the van der Waals interaction coefficient per unit area between two adjacent membranes (Wang et al., 2003, 2005).

The accuracy and efficiency of the simplified 3-membrane model (1) for a FLGS are justified by comparing its predictions with those given by an accurate multi-membrane model (presented in Appendix A). Our comparison (shown in Appendix B) confirms that the simplified 3-membrane model (1) exactly predicts vibration behavior of a 3- or 4-layer graphene sheet (with $m = 1$ or 2), while it gives reasonably accurate results for a 5- or 6- layer graphene sheet (with $m = 3$ or 4) of moderately larger length (e.g. $L/h > 100$). In all numerical examples shown below, the simplified 3-membane model (1) will be used to study flexural vibration of a tensioned FLGS (with $m = 1$ or 2) as an elastic metamaterial.

2.1. Free vibration of a FLGS

For free vibration of a FLGS with fixed ends and zero bending rigidity, the deflections w_1 and w_2 take the following form

$$\begin{Bmatrix} w_1(x,t) \\ w_2(x,t) \end{Bmatrix} = \sin\omega t \sum_{k=1}^{\infty} \begin{Bmatrix} A_k \\ B_k \end{Bmatrix} \sin\frac{k\pi x}{L} \tag{2}$$

with constants A_k and B_k ($k = 1, 2, 3,\ldots$). Substituting Eq. (2) into Eq. (1), we have

$$\begin{bmatrix} T\left(\frac{k\pi}{L}\right)^2 - \rho h\omega^2 + c & -c \\ -2c & \delta m T\left(\frac{k\pi}{L}\right)^2 - m\rho h\omega^2 + 2c \end{bmatrix} \begin{Bmatrix} A_k \\ B_k \end{Bmatrix} = \begin{Bmatrix} 0 \\ 0 \end{Bmatrix} \tag{3}$$

By setting the determinant of the coefficient matrix of Eq. (3) zero, all natural frequencies can be determined from the following eigen-equation.

$$\omega^4 - \left[\frac{(\delta+1)T}{\rho h}\left(\frac{k\pi}{L}\right)^2 + \frac{(m+2)c}{m\rho h}\right]\omega^2 + \frac{\delta T^2}{\rho^2 h^2}\left(\frac{k\pi}{L}\right)^4 + \frac{(\delta m+2)Tc}{m\rho^2 h^2}\left(\frac{k\pi}{L}\right)^2 = 0 \tag{4}$$

Please cite this article as: L. Lu, C.Q. Ru and X. Guo, Vibration isolation of few-layer graphene sheets, International Journal of Solids and Structures, https://doi.org/10.1016/j.ijsolstr.2019.08.029

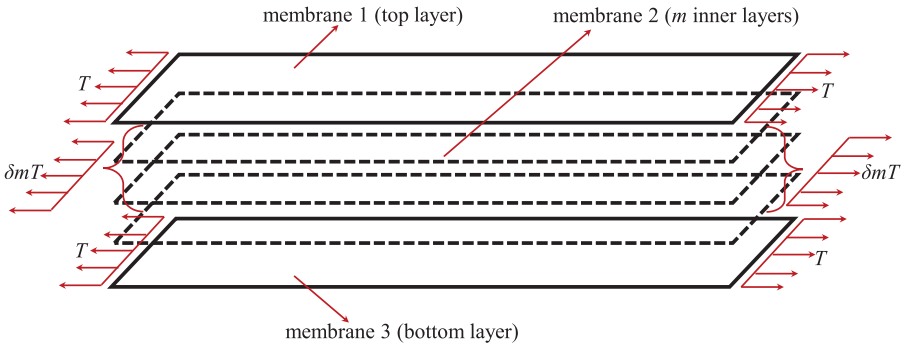

Fig. 1. Schematic of a tensioned few-layer graphene sheet modeled as a simplified 3-membrane system (The top and bottom layers are depicted in solid lines, and the m inner layers are depicted in dash lines).

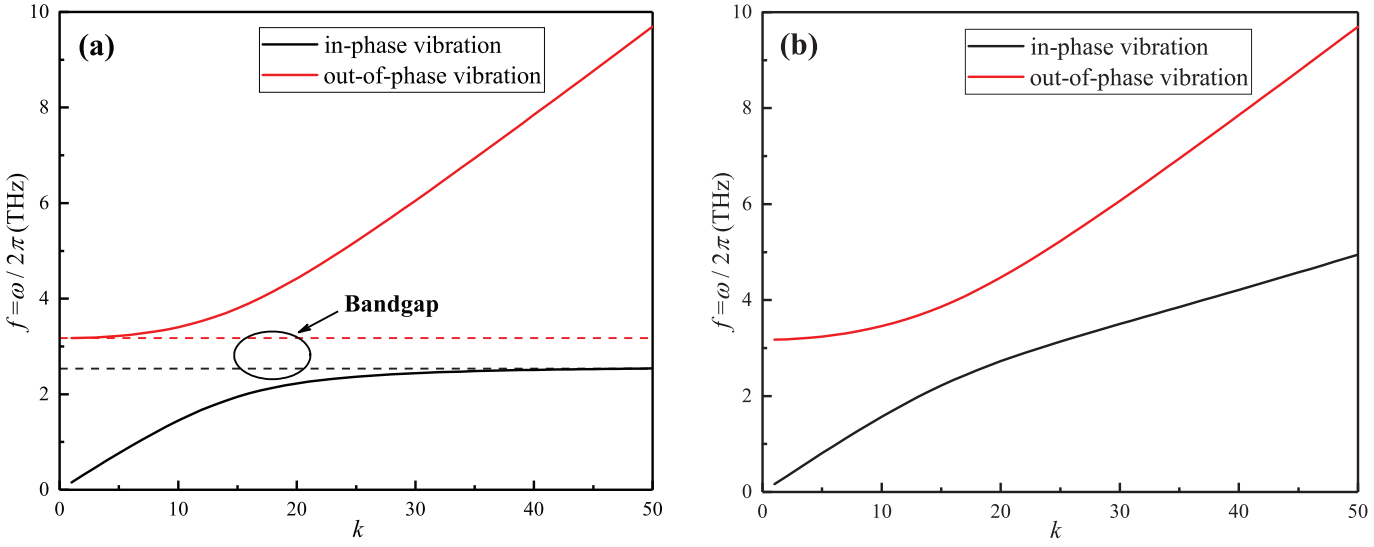

Fig. 2. Variation of natural frequencies of a tensioned 3-layer graphene sheet ($m=1$) with respect to the mode number k. (a) Tension-free inner layer ($\delta=0$). (b) Less-tensioned inner layer ($\delta=0.2$).

Fig. 2 shows the dependence of natural frequency $f\,(=\omega/2\pi)$ on the mode number k of a 3-layer graphene sheet ($m=1$) for $\delta=0$ and 0.2, respectively. The parameters $L=20\,h$ and $T=5$ N/m (corresponds to a tensile strain 1.5%, which is much smaller than the breaking strain 10–20% of graphene (Lee et al., 2008; Rasool et al., 2013)) are selected to demonstrate numerical results. It is seen from Fig. 2 that the natural frequencies are divided into a lower group and a higher group, and the lower group corresponds to essentially in-phase vibration of all layers while the higher group corresponds to essentially out-of-phase vibration between the outermost layers and the inner layer. In particular, for the case of tension-free inner layer with $\delta=0$, a bandgap exists between the lower group of natural frequencies and the higher group of natural frequencies, within which no natural frequency exists. When $\delta>0$ (e.g. $\delta=0.2$), however, the lower groups of natural frequencies approaches to infinity with increasing mode number k, which means that no bandgap exists between the lower group and the higher group of natural frequencies when $\delta>0$. Therefore, we shall focus on the case $\delta=0$ to define effective mass density and identify the associated bandgap.

2.2. Effective mass density of a FLGS

For a tensioned FLGS of tension-free inner layers ($\delta=0$), by eliminating w_2 from the two coupled Eq. (1), a single equation for the deflection of the outermost layer w_1 is obtained in the standard form of "wave equation" for a tensioned string

$$-2T\left(1+\frac{m\rho h}{2c}\frac{\partial^2}{\partial t^2}\right)\frac{\partial^2 w_1}{\partial x^2} + (m+2)\rho h\left[1+\frac{m\rho h}{(2+m)c}\frac{\partial^2}{\partial t^2}\right]\frac{\partial^2 w_1}{\partial t^2}=0 \tag{5}$$

Consider a periodic harmonic motion $w_1(x,\ t)=f(x)\exp(i\omega t)$, where $f(x)$ is the mode function, i is the imaginary unit, and ω denotes the circular frequency. Substituting this form of w_1 into Eq. (5), the governing equation for the deflection w_1 of a FLGS with $\delta=0$ can be written as

$$-2T\left(1-\frac{m\rho h\omega^2}{2c}\right)\frac{\partial^2 w_1}{\partial x^2}+(m+2)\rho h\left[1-\frac{m\rho h\omega^2}{(2+m)c}\right]\frac{\partial^2 w_1}{\partial t^2}=0 \tag{6}$$

In Eq. (6), $2T$ is the total tension force (per unit width) applied to the FLGS, and $(m+2)\rho h$ is the total mass density (per unit width) of the FLGS. Thus, effective mass density of the FLGS with tension-free inner layers ($\delta=0$) is given by

$$\rho_{eff}=\frac{1-\frac{m\rho h\omega^2}{(2+m)c}}{1-\frac{m\rho h\omega^2}{2c}}\rho \tag{7}$$

Thus, the effective mass density become negative when the frequency is inside the following bandgap

$$\omega_{\text{low}}=\sqrt{\frac{2c}{m\rho h}}<\omega<\sqrt{\frac{(m+2)c}{m\rho h}}=\sqrt{1+\frac{m}{2}}\omega_{\text{low}}=\omega_{\text{upp}} \tag{8}$$

Please cite this article as: L. Lu, C.Q. Ru and X. Guo, Vibration isolation of few-layer graphene sheets, International Journal of Solids and Structures, https://doi.org/10.1016/j.ijsolstr.2019.08.029

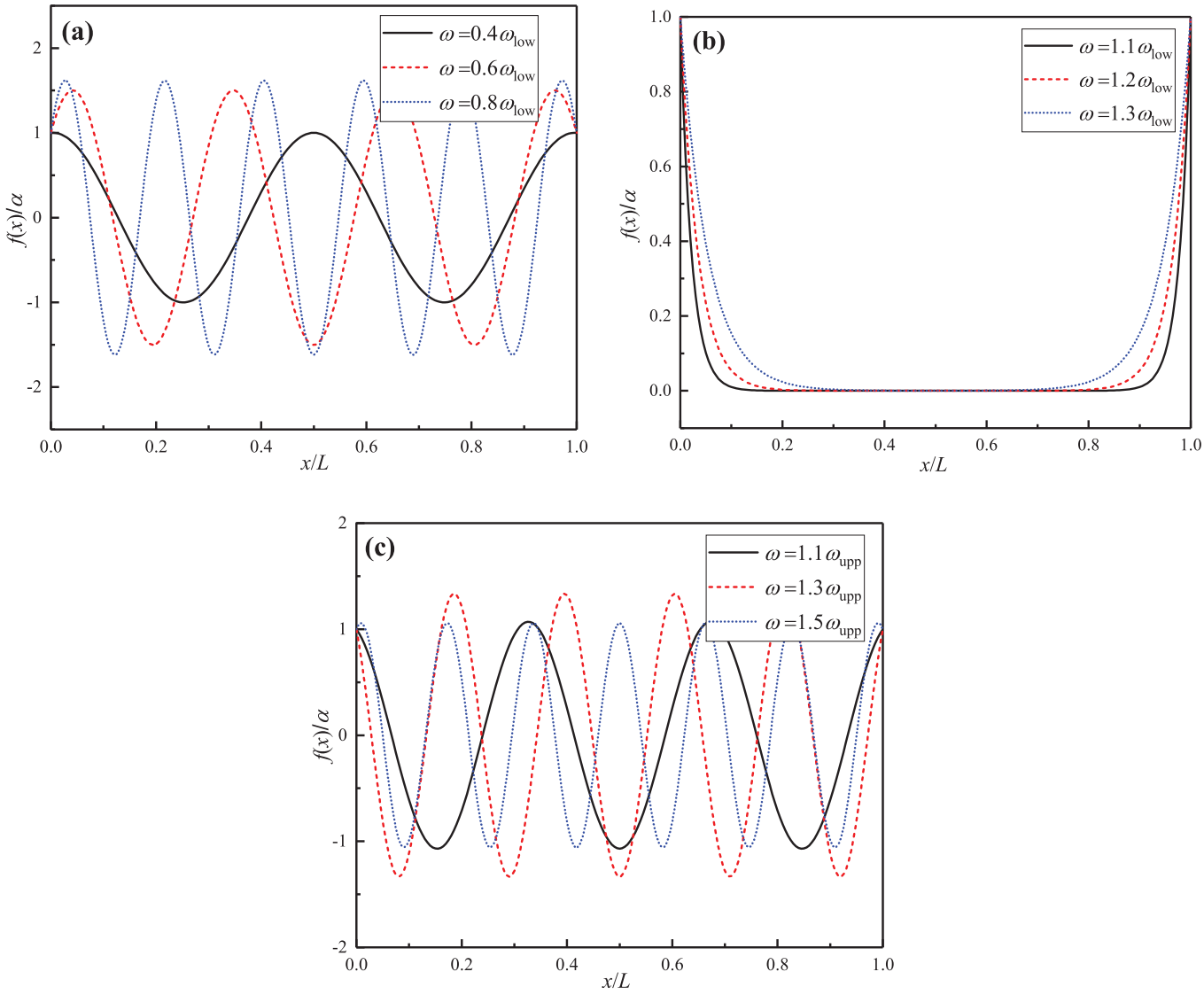

Fig. 3. Forced vibration mode of a 4-layer graphene sheet with tension-free inner layers ($\delta = 0$) driven by its vibrating ends under different excitation frequencies ω. (a) ω is below the bandgap (ω_{low}, ω_{upp}). (b) ω is within the bandgap (ω_{low}, ω_{upp}). (c) ω is above the bandgap (ω_{low}, ω_{upp}).

It turns out (as shown in Fig. 2(a)) that the lower edge of bandgap (8) is the upper limit for all natural frequencies associated with essentially in-phase vibration of all layers, and the upper edge of the bandgap (8) is the lower limit for all natural frequencies associated with essentially out-of-phase vibration between the outermost layers and the inner layers. In addition, it is seen that the width of the bandgap (8) is determined by the number of inner layers m, and the order of magnitude of bandgap frequencies of a FLGS is determined by the van der Walls interaction coefficient c between adjacent layers and falls in the terahertz range. In particular, the terahertz bandgap is independent of the geometry size of the FLGS. For example, the frequency bandgap is (2.59 THz, 3.17 THz) for a 3-layer graphene sheet ($m = 1$), and (1.83 THz, 2.59 THz) for a 4-layer graphene sheet ($m = 2$). It should be stated that terahertz vibration and wave propagation in nanomaterials and devices have been a major research topic of current interest (Juvé et al., 2010; Liu et al., 2013; Rahm et al., 2013; Al-Naib et al., 2015). It is expected that the present work can be helpful in design and analysis of terahertz metamaterials.

In what follows, we shall show that a FLGS with $\delta = 0$ does exhibit remarkable metamaterial behaviors within the bandgap (8), and even a FLGS with $\delta > 0$ can exhibit metamaterial-like behaviors in spite of the non-existence of a bandgap when $\delta > 0$.

3. Forced vibration of a few-layer graphene sheet

Vibration isolation is among the most important phenomena of elastic/acoustic metamaterials with potential application (Zhu et al., 2014; Jiang and He, 2017; Oh et al., 2017). In this section, two typical cases of forced vibration are considered to demonstrate remarkable vibration isolation of a tensioned FLGS as an elastic metamaterial. As stated above, forced vibration of nanoscale device or structures can be stimulated by external periodic stimulus at terahertz frequencies which can be much higher than their own natural frequencies. Therefore, it is of potential interest to investigate terahertz forced vibration of graphene-based nanoscale devices and structures even when their own natural frequencies are much below terahertz.

Please cite this article as: L. Lu, C.Q. Ru and X. Guo, Vibration isolation of few-layer graphene sheets, International Journal of Solids and Structures, https://doi.org/10.1016/j.ijsolstr.2019.08.029

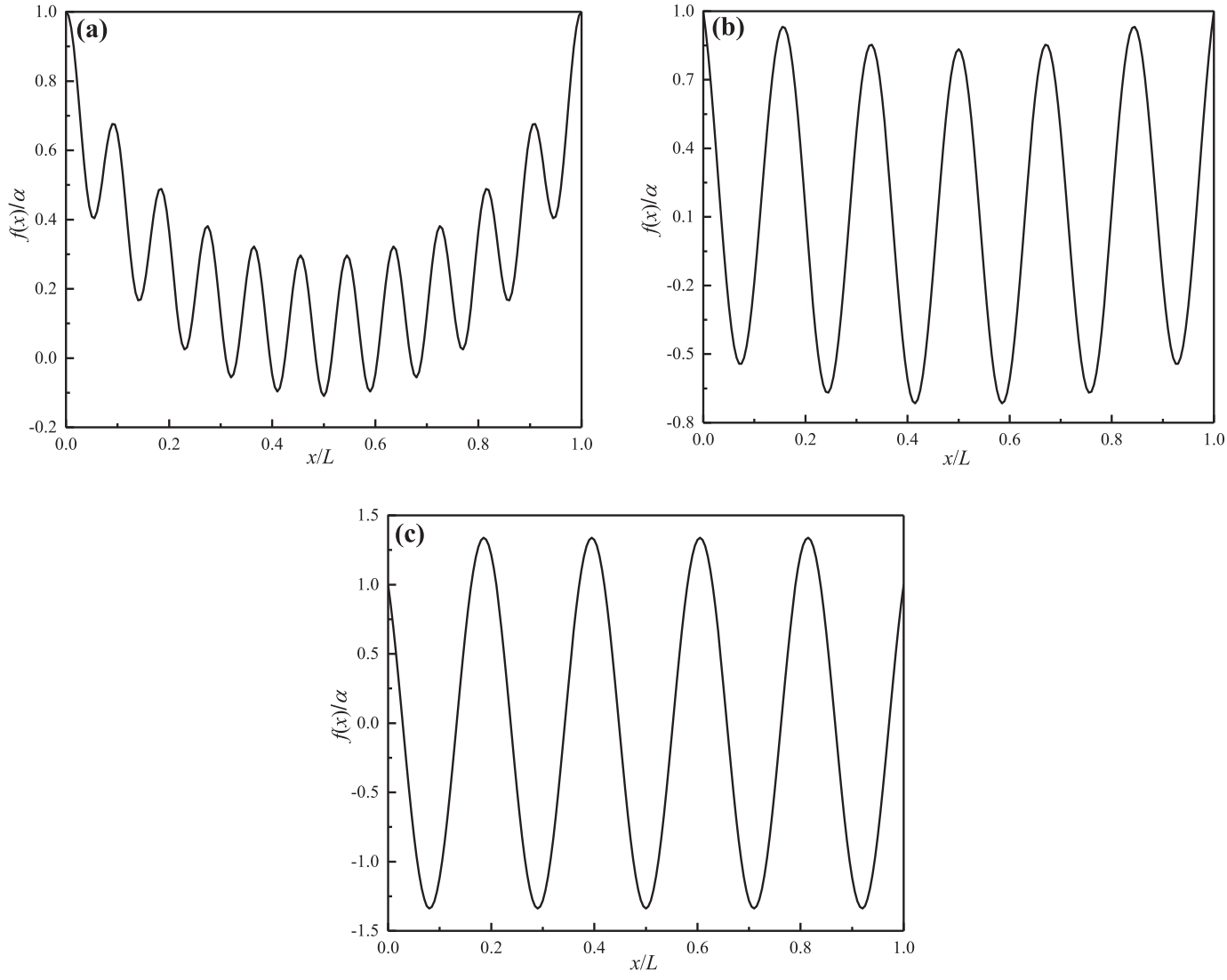

Fig. 4. Forced vibration mode of a 4-layer graphene sheet with tensioned inner layers driven by its vibrating ends under excitation frequency $\omega = 0.99\omega_{upp}$. (a) $\delta = 0.1$. (b) $\delta = 0.5$. (c) $\delta = 1$.

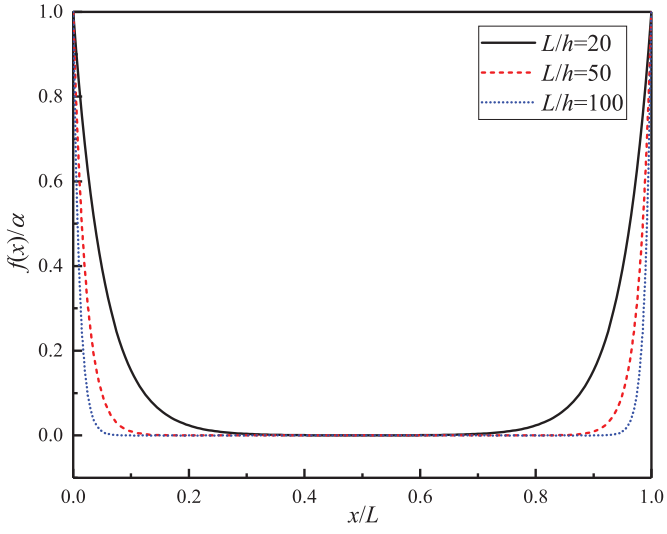

Fig. 5. Forced vibration mode of a 4-layer graphene sheet with tension-free inner layers ($\delta = 0$) and different length driven by its vibrating ends for $\omega = 1.3\omega_{low}$.

3.1. Forced vibration driven by vibrating ends

First, forced vibration of a tensioned FLGS driven by its periodically vibrating foundation which causes periodical vibration of its two ends will be studied. In this case, let us assume that $w_1 = w_2 = \alpha \sin\omega t$ at $x = 0$ and $x = L$, where α is the amplitude of the vibrating ends. The stimulated steady state forced vibration of the tensioned FLGS is of the form:

$$\begin{Bmatrix} w_1(x,t) \\ w_2(x,t) \end{Bmatrix} = \alpha \sin\omega t \left(1 + \sum_{k=1}^{\infty} \begin{Bmatrix} a_k \\ b_k \end{Bmatrix} \sin\frac{k\pi x}{L} \right) \tag{9}$$

in which a_k and b_k ($k = 1, 2, 3,\ldots$) are some real constants to be determined. Substituting w_1 and w_2 into Eq. (1), and using the Fourier series expansion

$$1 = \sum_{k=1}^{\infty} \frac{2[1 - \cos(k\pi)]}{k\pi} \sin\frac{k\pi x}{L}, 0 < x < L \tag{10}$$

One can obtain that

$$\begin{bmatrix} T\left(\frac{k\pi}{L}\right)^2 - \rho h\omega^2 + c & -c \\ -2c & \delta m T\left(\frac{k\pi}{L}\right)^2 - m\rho h\omega^2 + 2c \end{bmatrix} \begin{Bmatrix} a_k \\ b_k \end{Bmatrix}$$

Please cite this article as: L. Lu, C.Q. Ru and X. Guo, Vibration isolation of few-layer graphene sheets, International Journal of Solids and Structures, https://doi.org/10.1016/j.ijsolstr.2019.08.029

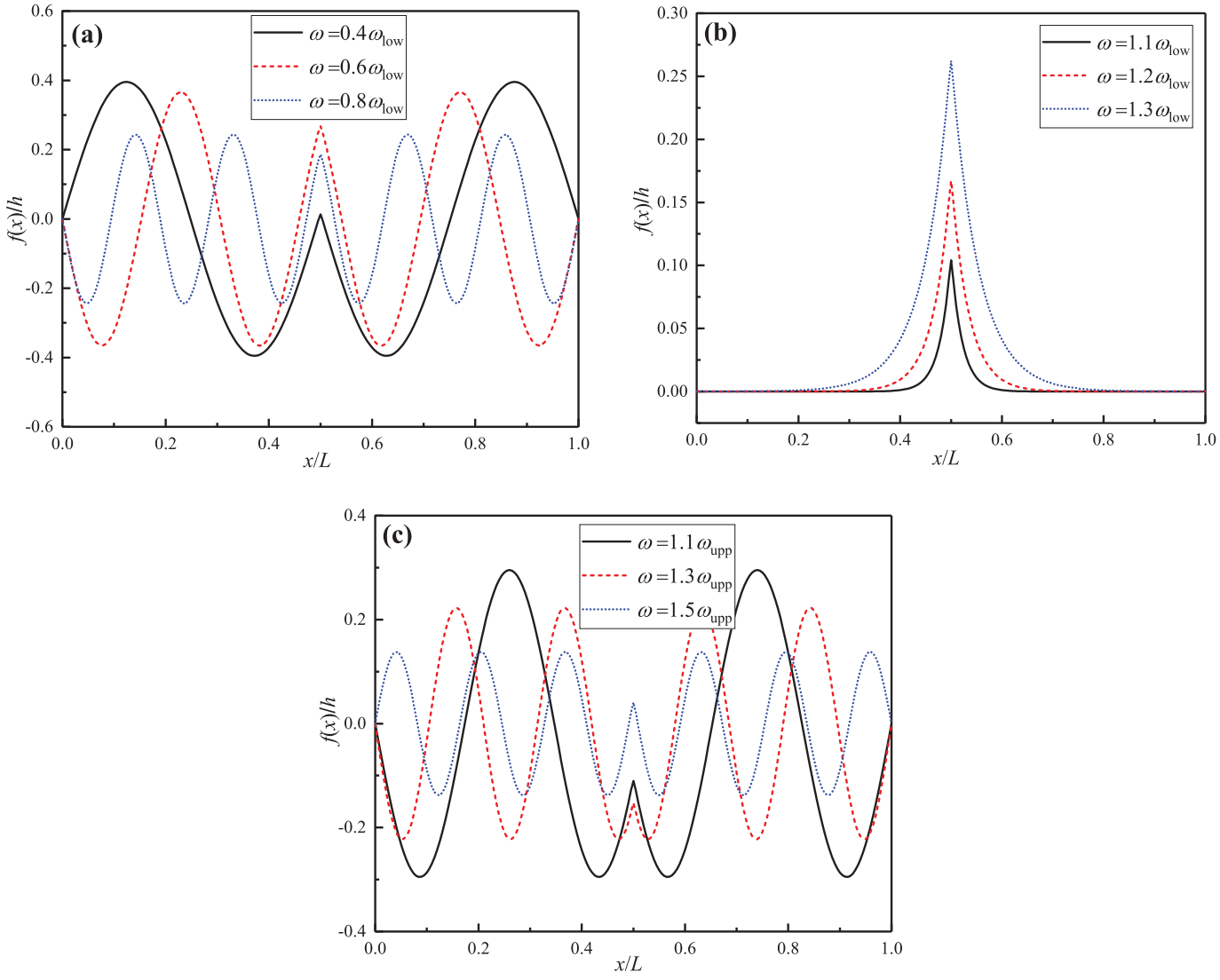

Fig. 6. Forced vibration mode of a 4-layer graphene sheet with tension-free inner layers ($\delta = 0$) driven by a point load under different excitation frequencies ω for $Q_0 = 5$ N/m. (a) ω is below the bandgap (ω_{low}, ω_{upp}). (b) ω is within the bandgap (ω_{low}, ω_{upp}). (c) ω is above the bandgap (ω_{low}, ω_{upp}).

$$= \begin{Bmatrix} 1 \\ m \end{Bmatrix} \rho h \omega^2 \frac{2[1-\cos(k\pi)]}{k\pi} \tag{11}$$

From Eq. (11), the coefficients a_k ($k = 1, 2, 3, \ldots$) of the outermost layers can be determined as

$$a_k = \frac{\rho h \omega^2 \left[\delta m T \left(\frac{k\pi}{L}\right)^2 - m\rho h \omega^2 + (m+2)c\right] \frac{2[1-\cos(k\pi)]}{k\pi}}{\left[T\left(\frac{k\pi}{L}\right)^2 - \rho h \omega^2 + c\right]\left[\delta m T \left(\frac{k\pi}{L}\right)^2 - m\rho h \omega^2 + 2c\right] - 2c^2} \tag{12}$$

Inserting the coefficients a_k into Eq. (9), the forced vibration of a tensioned FLGS driven by its periodically vibrating ends can be evaluated, as detailed in Section 4.1.

3.2. Forced vibration driven by an external periodic force

Next, forced vibration of a tensioned FLGS subjected to an external periodic force will be investigated. Consider an external periodic force $q(x,t) = q(x)\sin\omega t$ (per unit width) applied on the two outermost (top and bottom) layers of the FLGS. Thus, the governing Eq. (1) for the tensioned FLGS can be revised as

$$\begin{cases} -T\frac{\partial^2 w_1}{\partial x^2} + \rho h \frac{\partial^2 w_1}{\partial t^2} = c(w_2 - w_1) + q(x)\sin\omega t \\ -\delta m T \frac{\partial^2 w_2}{\partial x^2} + m\rho h \frac{\partial^2 w_2}{\partial t^2} = 2c(w_1 - w_2) \end{cases} \tag{13}$$

The external force $q(x)$ can always be expanded as

$$q(x) = \sum_{k=1}^{\infty} Q_k \sin\frac{k\pi x}{L}, \ (0 < x < L) \tag{14}$$

where Q_k is the Fourier coefficient determined by the given force distribution $q(x)$. For example, for a point load Q_0 applied at the midpoint $x = L/2$, we have

$$Q_k = \frac{2}{L} Q_0 \sin\frac{k\pi}{2}, \ (k = 1, 2, 3, \ldots) \tag{15}$$

The stimulated steady state forced vibration of the tensioned FLGS is of the form given by Eq. (2). Substituting Eqs. (2) and (14) into Eq. (13) yields

$$\begin{bmatrix} T\left(\frac{k\pi}{L}\right)^2 - \rho h \omega^2 + c & -c \\ -2c & \delta m T \left(\frac{k\pi}{L}\right)^2 - m\rho h \omega^2 + 2c \end{bmatrix} \begin{Bmatrix} A_k \\ B_k \end{Bmatrix} = \begin{Bmatrix} Q_k \\ 0 \end{Bmatrix} \tag{16}$$

Please cite this article as: L. Lu, C.Q. Ru and X. Guo, Vibration isolation of few-layer graphene sheets, International Journal of Solids and Structures, https://doi.org/10.1016/j.ijsolstr.2019.08.029

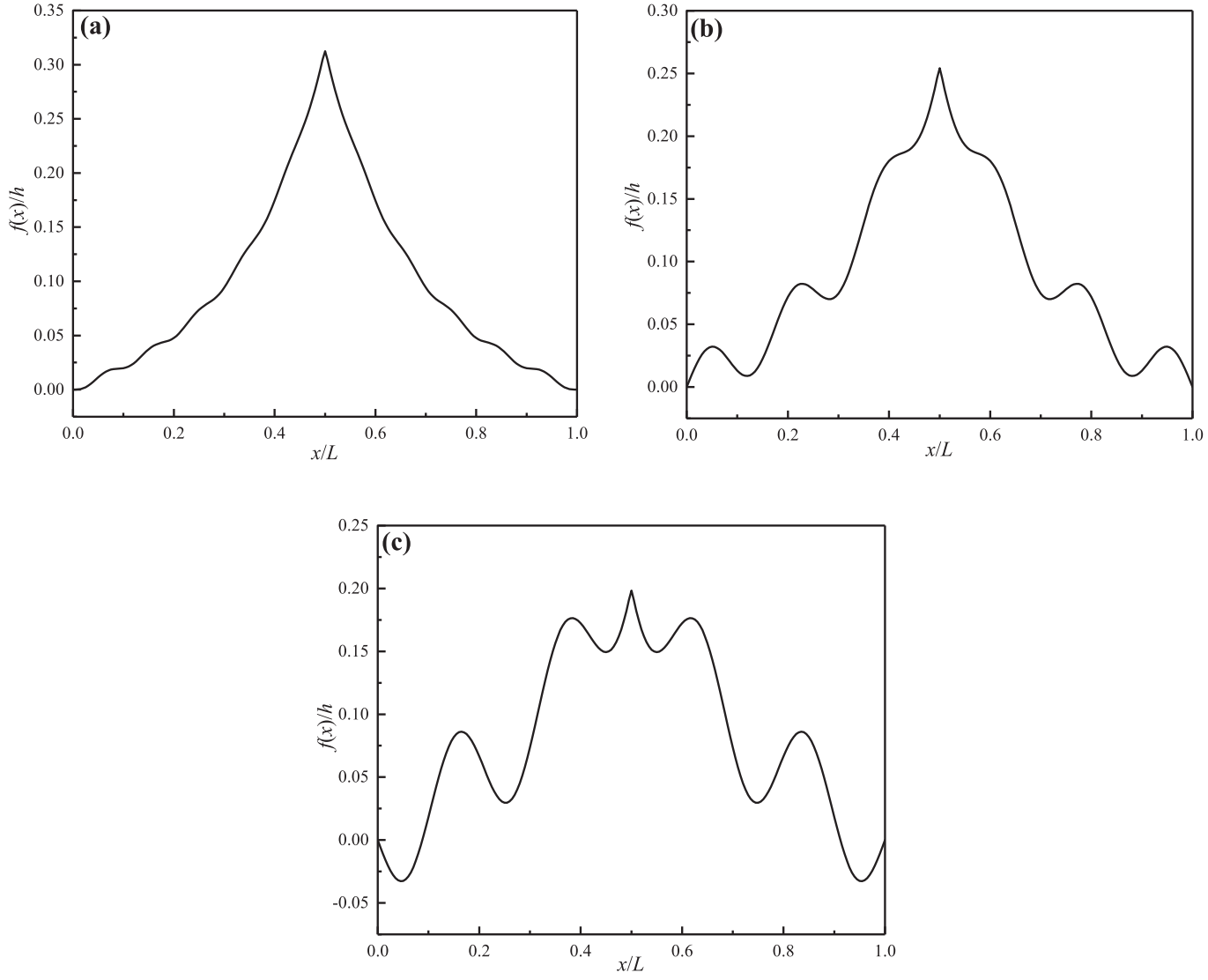

Fig. 7. Forced vibration mode of a 4-layer graphene sheet with tensioned inner layers driven by a point load applied at its midpoint under an excitation frequency $\omega = 0.99\omega_{upp}$ for $Q_0 = 2$ N/m. (a) $\delta = 0.1$. (b) $\delta = 0.5$. (c) $\delta = 1$.

From Eq. (16), the Fourier coefficient A_k of the outermost layers can be obtained as

$$A_k = \frac{\left[\delta mT\left(\frac{k\pi}{L}\right)^2 - m\rho h\omega^2 + 2c\right]Q_k}{\left[T\left(\frac{k\pi}{L}\right)^2 - \rho h\omega^2 + c\right]\left[\delta mT\left(\frac{k\pi}{L}\right)^2 - m\rho h\omega^2 + 2c\right] - 2c^2} \tag{17}$$

Substituting the coefficients A_k into Eq. (2), the forced vibration of a tensioned FLGS driven by an external force (such as a point force discussed here) can be evaluated, as detailed in Section 4.2.

4. Results and discussion

To demonstrate remarkable vibration isolation of a tensioned FLGS as an elastic metamaterial, a tensioned 4-layer graphene sheet ($m = 2$) is considered. The bandgap (ω_{low}, ω_{upp}) of a 4-layer graphene sheet is defined by the frequency bandgap (1.83 THz, 2.59 THz) and $\omega_{upp} = 1.41\omega_{low}$. Unless otherwise stated, we have $L = 20\,h$ and $T = 10$ N/m (corresponds to a tensile strain 2.9%, which is much smaller than the breaking strain 10–20% of graphene (Lee et al., 2008; Rasool et al., 2013)).

4.1. Vibration isolation of a few-layer graphene driven by vibrating ends

In Fig. 3, forced vibrational modes of a 4-layer graphene sheet ($m = 2$) with tension-free inner layers ($\delta = 0$) driven by its two vibrating ends are plotted. For the purpose of comparison, let us consider three cases: (a) excitation frequency below the bandgap, (b) excitation frequency within the bandgap, and (c) excitation frequency above the bandgap. It is seen from Fig. 3(b) that when the excitation frequency is within the bandgap, the forced vibrational mode is highly restricted to the two vibrating ends but vanishingly small in all other parts of the graphene sheet, in sharp contrast to the modes of excitation frequencies below or above the bandgap (see Fig. 3(a) and (c)) in which the forced vibrational mode always spreads into the entire graphene sheet.

Forced vibrational mode is shown in Fig. 4 for a 4-layer graphene sheet with tensioned inner layers ($\delta > 0$) driven by two vibrating ends with an excitation frequency close to the upper edge frequency of the bandgap (e.g. $\omega = 0.99\omega_{upp}$). It can be seen from Fig. 4(a) that when the inner layers of the graphene sheet are less-tensioned (e.g. $\delta = 0.1$), although the forced vibrational mode is not fully restricted to the two ends, its amplitude in the

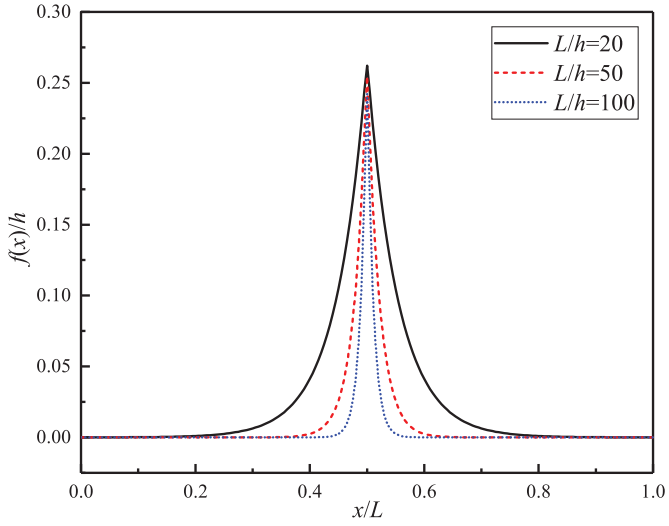

Fig. 8. Forced vibration mode of a 4-layer graphene sheet with tension-free inner layers ($\delta = 0$) and with different length driven by a point load for $Q_0 = 5$ N/m and $\omega = 1.3\omega_{\text{low}}$.

middle part of the graphene sheet is still much smaller than the amplitude of the two vibrating ends. This indicates that a few-layer graphene sheet with less-tensioned inner layers still exhibits similar vibration isolation behavior when the excitation frequency is close to the upper edge frequency of the bandgap (8) determined by tension-free inner layers with $\delta = 0$. However, such vibration isolation does disappear when the inner layer are equally-tensioned as the two outermost layers, as shown in Fig. 4(c).

To explore the dependence of the width of the localized mode on the length of graphene sheet, the forced vibrational modes of a 4-layer graphene sheet with tension-free inner layers driven by its vibrating ends are depicted in Fig. 5 for various length of the FLGS. It is seen from Fig. 5 that, for a given external excitation with excitation frequency within the bandgap, the width of localized vibrational mode for each of the two vibrating ends is about $6h$, independent of the length of the 4-layer graphene sheet, which indicates that the width of localized mode is essentially independent of the length of the graphene sheet.

4.2. Vibration isolation of a few-layer graphene driven by a point load

What shown in Fig. 6 is forced vibration mode of a 4-layer graphene sheet with tension-free inner layers driven by a point load applied at its midpoint. Similar as Fig. 3, we consider three cases of excitation frequencies, which are below, within and above the bandgap, respectively. It can be seen from Fig. 6(b) that for excitation frequency within the bandgap, the forced vibrational mode is highly localized near the midpoint where the external force is applied but vanishingly small in all other parts. In sharp contrast, for excitation frequency out of the bandgap (see Fig. 6(a) and (c)), the forced vibrational mode always spreads into the entire graphene sheet. Also, it can be seen from Fig. 6(b) that the maximum deflection of the tensioned graphene sheet gradually increases when the excitation frequency changes from the lower edge frequency to the upper edge frequency of the bandgap.

In Fig. 7, forced vibrational mode of a 4-layer graphene sheet with tensioned inner layers ($\delta > 0$), driven by a point load applied at its midpoint, is presented for an excitation frequency approaches to the upper edge frequency of the bandgap (e.g. $\omega = 0.99\omega_{\text{upp}}$). It is seen from Fig. 7(a) that when the inner layers of the graphene sheet are less-tensioned (e.g. $\delta = 0.1$), the deflection shows a sharp peak around the midpoint and quickly decays to two ends, and this phenomenon of vibration isolation gradually weakens with increasing tension force of the inner layers (see Fig. 7(b) and (c)), which indicates that vibration isolation essentially remains even for a FLGS of less-tensioned inner layers when the excitation frequency approaches to the upper edge frequency of the bandgap.

Fig. 8 plots the effect of length on the forced vibrational mode of a 4-layer graphene sheet with tension-free inner layers driven by a point load applied at its midpoint. Similar as the case of Fig. 5, the width of the localized mode around the midpoint is about 10 h for a given external force and excitation frequency within the bandgap, independent of the length of FLGS. Moreover, the maximum deflection is also nearly independent of the length of graphene sheet.

5. Conclusions

In this work, for the first time in literature, we showed that a tensioned few-layer graphene sheet exhibits negative effective mass in the terahertz range and behaves as an elastic metamaterial. Our main results include:

(1) A few-layer graphene sheet with two tensioned outermost layers and tension-free inner layers exhibits negative effective mass density within a specific bandgap.
(2) The order of magnitude of bandgap frequencies is determined by the van der Walls interaction coefficient between adjacent layers and falls in the terahertz range, and the width of the bandgap is determined by the number of inner layers.
(3) Such a few-layer graphene sheet with two tensioned outermost layers and tension-free inner layers exhibits remarkable vibration isolation, that is, when the external excitation frequency is within the bandgap, forced vibration will be highly restricted to a narrow region around the site of the applied excitation while all other parts of the graphene sheet remain essentially static.
(4) The phenomenon of vibration isolation remains qualitatively true even for a few-layer graphene sheets with highly tensioned outmost layers and less-tensioned inner layers.

It is expected that the results presented in this work can provide new insights into the design of graphene-based metamaterials and nano-resonators with potential application to terahertz vibration manipulating.

Acknowledgments

Lu and Guo thank the support from the National Natural Science Foundation of China (Grant nos. 11872233, 11472163), the China Scholarship Council (CSC), and the Innovation Program of Shanghai Municipal Education Commission, China (Grant no. 2017-01-07-00-09-E00019). Ru appreciates the support from the Natural Science and Engineering Research Council of Canada (NSERC-RGPIN204992).

Appendix A. An accurate multi-membrane model

An accurate multi-membrane model for multi-layer graphene sheets (MLGSs) is presented to verify the effectiveness and accuracy of the simplified 3-membrane model used in the present paper. Different than the simplified 3-membrane model which treats all inner layers together as a single membrane, the accurate multi-membrane model simulates a $(m+2)$-layer graphene sheet as a coupled $(m+2)$-membrane system. Thus, the governing equations

Please cite this article as: L. Lu, C.Q. Ru and X. Guo, Vibration isolation of few-layer graphene sheets, International Journal of Solids and Structures, https://doi.org/10.1016/j.ijsolstr.2019.08.029

for a $(m+2)$-layer graphene membrane can be written as

$$\begin{cases} -T\frac{\partial^2 w_1}{\partial x^2}+\rho h\frac{\partial^2 w_1}{\partial t^2}=c(w_2-w_1) \\ -\delta T\frac{\partial^2 w_2}{\partial x^2}+\rho h\frac{\partial^2 w_2}{\partial t^2}=c(w_3-w_2)-c(w_2-w_1) \\ \cdots\cdots\cdots \\ -\delta T\frac{\partial^2 w_{m+1}}{\partial x^2}+\rho h\frac{\partial^2 w_{m+1}}{\partial t^2}=c(w_{m+2}-w_{m+1})-c(w_{m+1}-w_m) \\ -T\frac{\partial^2 w_{m+2}}{\partial x^2}+\rho h\frac{\partial^2 w_{m+2}}{\partial t^2}=-c(w_{m+2}-w_{m+1}) \end{cases} \tag{A.1}$$

where w_1, w_2,..., w_{m+1}, w_{m+2} are the transverse deflection of first layer, second layer,..., $(m+1)$th layer and $(m+2)$th layer, respectively. Using a substitution method, Eq. (A.1) can be rewritten into a single equation for the deflection w_1 of the top layer, and thus the effective mass density can be defined and discussed when $\delta=0$. Here, let us consider a tensioned few-layer graphene sheet (FLGS) with total 3 to 6 layers.

It can be verified that vibration modes of a FLGS, with total $(m+2)$ layers, can be classified into two classes: "bending modes" characterized by the in-phase condition "$w_1=w_{m+2}$" of the two outermost layers, and "sausage-modes" characterized by the anti-phase condition "$w_1=-w_{m+2}$" of the two outermost layers. Since the present paper focuses on flexural vibration, we shall only consider vibration modes characterized by the in-phase condition "$w_1=w_{m+2}$" of the two outermost layers. For a 3- or 4-layer graphene sheet ($m=1$ or 2), it can be easily verified that Eq. (A.1) with the in-phase condition $w_1=w_3$ of the two outermost layers will be exactly reduced to the simplified 3-membrane model (1). Therefore, in what follows, let us discuss a 5-layer ($m=3$) and 6-layer ($m=4$) graphene sheet, respectively.

Appendix A.1. 5-membrane model

For a 5-layer graphene sheet, it can be easily verified that the in-phase condition "$w_1=w_5$" of the two outermost layers leads to $w_2=w_4$. Thus, Eq. (A.1) is reduced to 3 equations for (w_1, w_2, w_3) as follows

$$\begin{cases} -T\frac{\partial^2 w_1}{\partial x^2}+\rho h\frac{\partial^2 w_1}{\partial t^2}=c(w_2-w_1) \\ -\delta T\frac{\partial^2 w_2}{\partial x^2}+\rho h\frac{\partial^2 w_2}{\partial t^2}=c(w_3-w_2)-c(w_2-w_1) \\ -\delta T\frac{\partial^2 w_3}{\partial x^2}+\rho h\frac{\partial^2 w_3}{\partial t^2}=2c(w_2-w_3) \end{cases} \tag{A.2}$$

Since the effective mass density can be defined only when $\delta=0$, let us consider the case $\delta=0$. When $\delta=0$, eliminating w_2 and w_3, the governing equation for w_1 can be obtained as

$$-2T\left(1+\frac{2\rho h}{c}\frac{\partial^2}{\partial t^2}+\frac{\rho^2h^2}{2c^2}\frac{\partial^4}{\partial t^4}\right)\frac{\partial^2 w_1}{\partial x^2} +5\rho h\left(1+\frac{\rho h}{c}\frac{\partial^2}{\partial t^2}+\frac{\rho^2h^2}{5c^2}\frac{\partial^4}{\partial t^4}\right)\frac{\partial^2 w_1}{\partial t^2}=0 \tag{A.3}$$

Substituting $w_1(x,\ t)=f(x)\exp(i\omega t)$ into Eq. (A.3), the effective mass density for a 5-layer graphene sheet with highly tensioned outmost layer but tension-free inner layers ($\delta=0$) can be written as

$$\rho_{eff}=\frac{1-\frac{\rho h\omega^2}{c}+\frac{\rho^2h^2\omega^4}{5c^2}}{1-\frac{2\rho h\omega^2}{c}+\frac{\rho^2h^2\omega^4}{2c^2}}\rho \tag{A.4}$$

Now let us discuss forced vibration for general case with $\delta\geq 0$. First, for forced vibration driven by periodically vibrating ends, the deflections take the forms as

$$\begin{Bmatrix} w_1 \\ w_2 \\ w_3 \end{Bmatrix}=\alpha\sin\omega t\left(1+\sum_{k=1}^{\infty}\begin{Bmatrix} a_k \\ b_k \\ c_k \end{Bmatrix}\sin\frac{k\pi x}{L}\right) \tag{A.5}$$

Substituting the deflections w_1, w_2 and w_3 into Eq. (A.2) and using the Fourier series expansion Eq. (7) yield

$$\begin{bmatrix} P & -c & 0 \\ -c & Q & -c \\ 0 & -2c & Q \end{bmatrix}\begin{Bmatrix} a_k \\ b_k \\ c_k \end{Bmatrix}=\begin{Bmatrix} M \\ M \\ M \end{Bmatrix} \tag{A.6}$$

where

$$P=T\left(\frac{k\pi}{L}\right)^2-\rho h\omega^2+c,\ Q=\delta T\left(\frac{k\pi}{L}\right)^2-\rho h\omega^2+2c,$$
$$M=\rho h\omega^2\frac{2[1-\cos(k\pi)]}{k\pi} \tag{A.7}$$

By solving the matrix Eq. (A.6), a_k can be obtained as

$$a_k=\frac{(Q^2+cQ-c^2)M}{PQ^2-2Pc^2-Qc^2} \tag{A.8}$$

Next, for forced vibration driven by an external force, the deflections are taken as

$$\begin{Bmatrix} w_1 \\ w_2 \\ w_3 \end{Bmatrix}=\sin\omega t\sum_{k=1}^{\infty}\begin{Bmatrix} A_k \\ B_k \\ C_k \end{Bmatrix}\sin\frac{k\pi x}{L} \tag{A.9}$$

Substituting the expressions of w_1, w_2 and w_3 into Eq. (A.2), and considering the same external force as Eq. (14), one can obtain that

$$\begin{bmatrix} P & -c & 0 \\ -c & Q & -c \\ 0 & -2c & Q \end{bmatrix}\begin{Bmatrix} A_k \\ B_k \\ C_k \end{Bmatrix}=\begin{Bmatrix} Q_k \\ 0 \\ 0 \end{Bmatrix} \tag{A.10}$$

The coefficient A_k can be determined by solving the matrix Eq. (A.10), as

$$A_k=\frac{(Q^2-2c^2)Q_k}{PQ^2-2Pc^2-Qc^2} \tag{A.11}$$

Appendix A.2. 6-membrane model

Similarly, for a 6-layer graphene sheet, considering the in-phase condition $w_1=w_6$ of the two outermost layers leads to $w_2=w_5$ and $w_3=w_4$. Thus, Eq. (A.1) can be exactly reduced to 3 equations for (w_1, w_2, w_3) as

$$\begin{cases} -T\frac{\partial^2 w_1}{\partial x^2}+\rho h\frac{\partial^2 w_1}{\partial t^2}=c(w_2-w_1) \\ -\delta T\frac{\partial^2 w_2}{\partial x^2}+\rho h\frac{\partial^2 w_2}{\partial t^2}=c(w_3-w_2)-c(w_2-w_1) \\ -\delta T\frac{\partial^2 w_3}{\partial x^2}+\rho h\frac{\partial^2 w_3}{\partial t^2}=c(w_2-w_3) \end{cases} \tag{A.12}$$

When $\delta=0$, the governing equation for w_1 can be obtained from Eq. (A.12) as

$$-T\left(1+\frac{3\rho h}{c}\frac{\partial^2}{\partial t^2}+\frac{\rho^2h^2}{c^2}\frac{\partial^4}{\partial t^4}\right)\frac{\partial^2 w_1}{\partial x^2} +3\rho h\left(1+\frac{4\rho h}{3c}\frac{\partial^2}{\partial t^2}+\frac{\rho^2h^2}{3c^2}\frac{\partial^4}{\partial t^4}\right)\frac{\partial^2 w_1}{\partial t^2}=0 \tag{A.13}$$

Inserting $w_1=f(x)\exp(i\omega t)$ into Eq. (A.13), the effective mass density of a 6-layer graphene sheet with highly tensioned outmost layer but tension-free inner layers ($\delta=0$) is given by

$$\rho_{eff}=\frac{1-\frac{4\rho h\omega^2}{3c}+\frac{\rho^2h^2\omega^4}{3c^2}}{1-\frac{3\rho h\omega^2}{c}+\frac{\rho^2h^2\omega^4}{c^2}}\rho \tag{A.14}$$

For general case with $\delta\geq 0$, substituting Eq. (A.5) into Eq. (A.12), the governing equations for forced vibration driven by vibrating ends can be achieved as

$$\begin{bmatrix} P & -c & 0 \\ -c & Q & -c \\ 0 & -c & R \end{bmatrix}\begin{Bmatrix} a_k \\ b_k \\ c_k \end{Bmatrix}=\begin{Bmatrix} M \\ M \\ M \end{Bmatrix} \tag{A.15}$$

Please cite this article as: L. Lu, C.Q. Ru and X. Guo, Vibration isolation of few-layer graphene sheets, International Journal of Solids and Structures, https://doi.org/10.1016/j.ijsolstr.2019.08.029

where P, Q and M have been defined in Eq. (A.7), R is defined as

$$R = \delta T\left(\frac{k\pi}{L}\right)^2 - \rho h\omega^2 + c \tag{A.16}$$

From Eq. (A.15), the coefficients a_k for w_1 can be given by

$$a_k = \frac{(c+Q)MR}{PQR-(P+R)c^2} \tag{A.17}$$

Substituting Eq. (A.9) into Eq. (A.12), and considering the same external force as Eq. (14), the governing equations for forced vibration driven by an external force can be rewritten as

$$\begin{bmatrix} P & -c & 0 \\ -c & Q & -c \\ 0 & -c & R \end{bmatrix}\begin{Bmatrix} A_k \\ B_k \\ C_k \end{Bmatrix} = \begin{Bmatrix} Q_k \\ 0 \\ 0 \end{Bmatrix} \tag{A.18}$$

Thus, the coefficient A_k can be determined as

$$A_k = \frac{(QR-c^2)Q_k}{PQR-Pc^2-Rc^2} \tag{A.19}$$

Appendix B. Validation of the simplified 3-membrane model

Let us verify the effectiveness and accuracy of the simplified 3-membrane model used in the present paper which treats all inner layers together as a single elastic membrane. For this purpose, let us consider the case $\delta = 0$, and verify the results given by the simplified 3-membrane model (1) by the accurate multi-membrane model (A.1).

Table B.1
Comparison of the lowest bandgap frequencies (THz) and the normalized bandgap width predicted by the simplified 3-membrane model and the multi-membrane model when $\delta = 0$. ($f_{low} = \omega_{low}/(2\pi)$, $f_{upp} = \omega_{upp}/(2\pi)$).

		f_{low}	Diff.	f_{upp}	Diff.	$\Delta f / f_{low}$
$m=1$	Multi-membrane model	2.59	–	3.17	–	0.22
	3-membrane model	2.59	0	3.17	0	
$m=2$	Multi-membrane model	1.83	–	2.59	–	0.42
	3-membrane model	1.83	0	2.59	0	
$m=3$	Multi-membrane model	1.40	–	2.15	–	0.54
	3-membrane model	1.50	7.1%	2.36	9.8%	0.57
$m=4$	Multi-membrane model	1.13	–	1.83	–	0.62
	3-membrane model	1.29	14%	2.24	22%	0.74

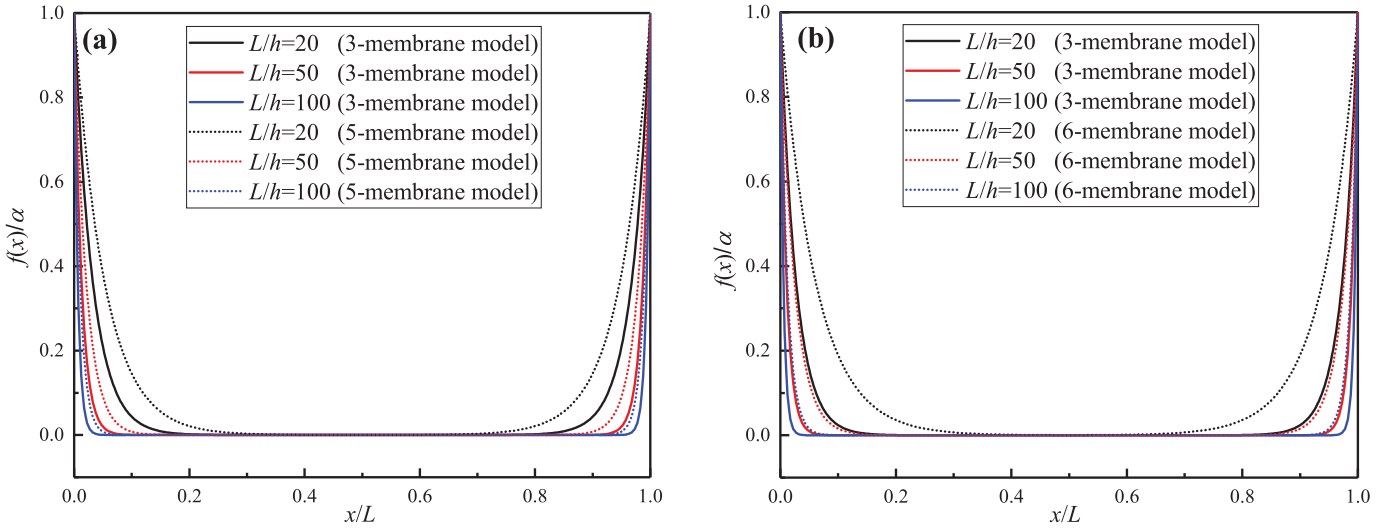

Fig. B.1. Comparisons of the forced vibrational mode driven by two vibrating ends given by the simplified 3-membrane model and the accurate multi-membrane model for $\delta = 0$ and $T = 5$ N/m. (a) 5-layer graphene sheet under an excitation frequency $\omega = 4\pi$ THz. (b) 6-layer graphene sheet under an excitation frequency $\omega = 3.4\pi$ THz.

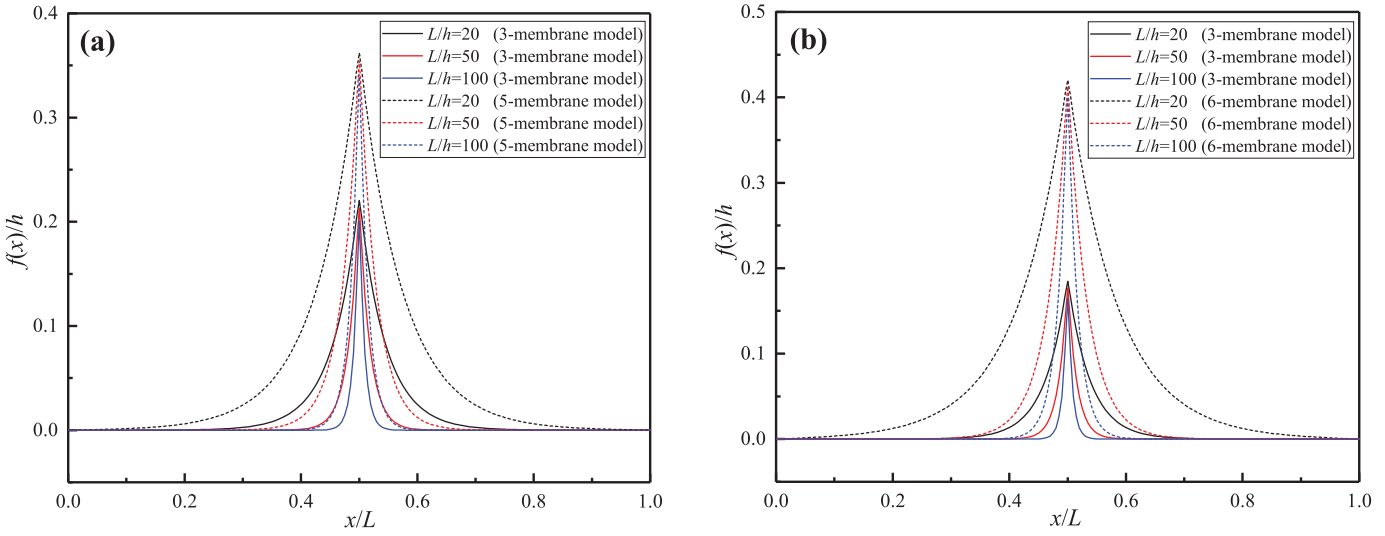

Fig. B.2. Comparisons of the forced vibrational mode driven by a point load given by the simplified 3-membrane model and the accurate multi-membrane model with $\delta = 0$, $Q_0 = 5$ N/m and $T = 10$ N/m. (a) 5-layer graphene sheet under an excitation frequency $\omega = 4\pi$ THz. (b) 6-layer graphene sheet under an excitation frequency $\omega = 3.4\pi$ THz.

Please cite this article as: L. Lu, C.Q. Ru and X. Guo, Vibration isolation of few-layer graphene sheets, International Journal of Solids and Structures, https://doi.org/10.1016/j.ijsolstr.2019.08.029

In Table B.1, the edge frequencies of the lowest bandgap predicted by the simplified 3-membrane model are compared with those obtained by the accurate multi-membrane model when $\delta = 0$. It is seen from Table B.1 that the simplified 3-membrane model exactly predict the bandgap of a 3- or 4-layer graphene sheet ($m = 1$ or 2). For graphene sheets more than 4 layers (say, $m = 3$ and 4), however, the bandgap given by the simplified 3-membrane model is a little higher (about 10–20%) than that given by the accurate multi-membrane model, and the difference between the bandgaps given by the two models increases with increasing number of layers. Also, it is found that the normalized bandgap width increases as the number of inner layer increases for both multi-membrane model and simplified membrane model, as expected.

To further examine the accuracy of the simplified 3-membrane model, detailed comparison between the forced vibrational modes of a 5- and a 6- layer graphene sheet with $\delta = 0$ given by the two models, driven by two vibrating ends or a point load, are made in Figs. B.1 and B.2 for an excitation frequency within the bandgap. From all figures shown here, it is seen that the deflections predicted by the simplified 3-membrane model is a little lower than that predicted by the accurate multi-membrane model, and the discrepancy between the results given by the two modes gradually decreases with increasing length of the graphene sheets. In summary, the present simplified 3-membrane model exactly predict the bandgap of a 3- or 4-layer graphene sheet ($m = 1$ or 2), while it gives reasonably accurate results for a 5- or 6-layer graphene sheet with a larger length (e.g. $L/h > 100$). This justifies the effectiveness and reasonable accuracy of the simplified 3-membrane model for FLGS.

References

Al-Naib, I., Sipe, J.E., Dignam, M.M., 2015. Nonperturbative model of harmonic generation in undoped graphene in the terahertz regime. New J. Phys. 17, 113018.
Atalaya, J., Isacsson, A., Kinaret, J.M., 2008. Continuum elastic modeling of graphene resonators. Nano Lett. 8, 4196–4200.
Beli, D., Arrudaa, J.R.F., Ruzzene, M., 2018. Wave propagation in elastic metamaterial beams and plates with interconnected resonators. Int. J. Solids Struct. 139-140, 105–120.
Bunch, J.S., van der Zande, A.M., Verbridge, S.S., Frank, I.W., Tanenbaum, D.M., Parpia, J.M., Craighead, H.G., McEuen, P.L., 2007. Electromechanical resonators from graphene sheets. Science 315, 490–492.
Castellanos-Gomez, A., Singh, V., van der Zant, H.S.J., Steele, G.A., 2015. Mechanics of freely-suspended ultrathin layered materials. Ann. Phys. (Berlin) 527, 27–44.
Castro Neto, A.H., Guinea, F., Peres, N.M.R., Novoselov, K.S., Geim, A.K., 2009. The electronic properties of graphene. Rev. Mod. Phys. 81, 109.
Chang, I.L., Liang, Z.X., Kao, H.W., Chang, S.H., Yang, C.Y., 2018. The wave attenuation mechanism of the periodic local resonant metamaterial. J. Sound Vib. 412, 349–359.
Chen, C., Rosenblatt, S., Bolotin, K.I., Kalb, W., Kim, P., Kymissis, I., Stormer, H.L., Heinz, T.F., Hone, J., 2009. Performance of monolayer graphene nanomechanical resonators with electrical readout. Nat. Nanotechnol. 4, 861–867.
Chen, Y.Y., Hu, G.K., Huang, G.L., 2017. A hybrid elastic metamaterial with negative mass density and tunable bending stiffness. J. Mech. Phys. Solids 105, 179–198.
Dienwiebel, M., Verhoeven, G.S., Pradeep, N., Frenken, J.W.M., 2004. Superlubricity of graphite. Phys. Rev. Lett. 92, 126101.
Frank, I.W., Tanenbaum, D.M., van der Zande, A.M., McEuen, P.L., 2007. Mechanical properties of suspended graphene sheets. J. Vac. Sci. Technol. B 25, 2558–2561.
Garcia-Sanchez, D., van der Zande, A.M., Paulo, A.S., Lassagne, B., McEuen, P.L., Bachtold, A., 2008. Imaging mechanical vibrations in suspended graphene sheets. Nano Lett. 8, 1399–1403.
Han, J., Ryu, S., Kim, D.K., Woo, W., Sohn, D., 2016. Effect of interlayer sliding on the estimation of elastic modulus of multilayer graphene in nanoindentation simulation. EPL 114, 68001.
Hao, Y., Wang, Y., Wang, L., Ni, Z., Wang, Z., Wang, R., Koo, C.K., Shen, Z., Thong, J.T.L., 2010. Probing layer number and stacking order of few-layer graphene by Raman spectroscopy. Small 6, 195–200.
Huang, H.H., Sun, C.T., Huang, G.L., 2009. On the negative effective mass density in acoustic metamaterials. Int. J. Eng. Sci. 47, 610–617.
Jnawali, G., Rao, Y., Yan, H., Heinz, T.F., 2013. Observation of a transient decrease in terahertz conductivity of single-layer graphene induced by ultrafast optical excitation. Nano Lett. 13, 524–530.
Jiang, T., He, Q., 2017. Dual-directionally tunable metamaterial for low-frequency vibration isolation. Appl. Phys. Lett. 110, 021907.
Juvé, V., Crut, A., Maioli, P., Pellarin, M., Broyer, M., Del Fatti, N., Vallée, F., 2010. Probing elasticity at the nanoscale: terahertz acoustic vibration of small metal nanoparticles. Nano Lett. 10, 1853–1858.
Khan, Z.H., Kermany, A.R., Öchsner, A., Iacopi, F., 2017. Mechanical and electromechanical properties of graphene and their potential application in MEMS. J. Phys. D Appl. Phys. 50, 053003.
Koshino, M., 2015. Interlayer interaction in general incommensurate atomic layers. New J. Phys. 17, 015014.
Kumar, N., Kumar, J., Gerstenkorn, C., Wang, R., Chiu, H.Y., Smir, A.L., Zhao, H., 2013. Third harmonic generation in graphene and few-layer graphite films. Phys. Rev. B 87 (12), 121406.
Lee, C., Wei, X., Kysar, J.W., Hone, J., 2008. Measurement of the elastic properties and intrinsic strength of monolayer graphene. Science 321, 385–388.
Lee, S.H., Wright, O.B., 2016. Origin of negative density and modulus in acoustic metamaterials. Phys. Rev. B 93, 024302.
Lewinska, M.A., Kouznetsova, V.G., van Dommelena, J.A.W., Krushynska, A.O., Geers, M.G.D., 2017. The attenuation performance of locally resonant acoustic metamaterials based on generalised viscoelastic modelling. Int. J. Solids Struct. 126-127, 163–174.
Liu, X.Y., Wang, F.C., Wu, H.A., 2013. Anisotropic propagation and upper frequency limitation of terahertz waves in graphene. Appl. Phys. Lett. 103, 071904.
Liu, Z.Y., Chan, C.T., Sheng, P., 2005. Analytic model of phononic crystals with local resonances. Phys. Rev. B 71, 014103.
Liu, Z.Y., Zhang, X.X., Mao, Y.W., Zhu, Y.Y., Yang, Z.Y., Chan, C.T., Sheng, P., 2000. Locally resonant sonic materials. Science 289, 1734–1736.
Li, Y., Baker, E., Reissman, T., Sun, C., Liu, W.K., 2017. Design of mechanical metamaterials for simultaneous vibration isolation and energy harvesting. Appl. Phys. Lett. 111, 251903.
Li, Z., Wang, X., 2016. On the dynamic behavior of a two-dimensional elastic metamaterial system. Int. J. Solids Struct. 78-79, 174–181.
Lui, C.H., Malard, L.M., Kim, S.H., Lantz, G., Laverge, F.E., Saito, R., Heinz, T.F., 2012. Observation of layer-breathing mode vibrations in few-layer graphene through combination Raman scattering. Nano Lett. 12, 5539–5544.
Lu, L., Ru, C.Q., Guo, X.M., 2017. Vibration of a multilayer graphene sheet under layerwise tension forces. Int. J. Mech. Sci. 121, 157–163.
Ma, G., Sheng, P., 2016. Acoustic metamaterials: from local resonances to broad horizons. Sci. Adv. 2, e1501595.
Milton, G.W., Willis, J.R., 2007. On modifications of Newton's second law and linear continuum elastodynamics. Proc. R. Soc. A 463, 855–880.
Oh, J.H., Qi, S., Kim, Y.Y., Assouar, B., 2017. Elastic metamaterial insulator for broadband low-frequency flexural vibration shielding. Phys. Rev. Appl. 8, 054034.
Oudich, M., Li, Y., 2017. Tunable sub-wavelength acoustic energy harvesting with a metamaterial plate. J. Phys. D Appl. Phys. 50, 315104.
Poot, M., van der Zant, H.S.J., 2008. Nanomechanical properties of few-layer graphene membranes. Appl. Phys. Lett. 92, 063111.
Rahm, M., Li, J.S., Padilla, W.J., 2013. THz wave modulators: a brief review on different modulation techniques. J. Infrared Millim. Terahertz Waves 34, 1–27.
Rasool, H.I., Ophus, C., Klug, W.S., Zettl, A., Gimzewski, J.K., 2013. Measurement of the intrinsic strength of crystalline and polycrystalline graphene. Nat. Commun. 4, 2811.
Ren, L., Zhang, Q., Yao, J., Sun, Z., Kaneko, R., Yan, Z., Nanot, S., Jin, Z., Kawayama, I., Tonouchi, M., Tour, J.M., Kono, J., 2012. Terahertz and infrared spectroscopy of gated large-area graphene. Nano Lett. 12, 3711–3715.
Svintsov, D., Leiman, V.G., Ryzhii, V., Otsuji, T., Shur, M.S., 2014. Graphene nanoelectromechanical resonators for the detection of modulated terahertz radiation. J. Phys. D Appl. Phys. 47, 505105.
Wang, C.Y., Ru, C.Q., Mioduchowski, A., 2003. Axially compressed buckling of pressured multiwall carbon nanotubes. Int. J. Solids Struct. 40, 3893–3911.
Wang, C.Y., Ru, C.Q., Mioduchowski, A., 2005. Axisymmetric and beamlike vibrations of multiwall carbon nanotubes. Phys. Rev. B 72, 075414.
Wang, L., Chen, X., Yu, A., Zhang, Y., Ding, J., Lu, W., 2014. Highly sensitive and wide-band tunable terahertz response of plasma waves based on graphene field effect transistors. Sci. Rep. 4, 5470.
Wang, X., 2014. Dynamic behaviour of a metamaterial system with negative mass and modulus. Int. J. Solids Struct. 51, 1534–1541.
Xu, L., Ma, T., Hu, Y., Wang, H., 2012. Molecular dynamics simulation of the interlayer sliding behavior in few-layer graphene. Carbon 50, 1025–1032.
Yang, Z., Mei, J., Yang, M., Chan, N.H., Sheng, P., 2008. Membrane-type acoustic metamaterial with negative dynamic mass. Phys. Rev. Lett. 101, 204301.
Yao, S.S., Zhou, X.M., Hu, G.K., 2008. Experimental study on negative effective mass in a 1D mass-spring system. New J. Phys. 10, 043020.
van der Zande, A.M., Barton, R.A., Alden, J.S., Ruiz-Vargas, C.S., Whitney, W.S., Pham, P.H.Q., Park, J., Parpia, J.M., Craighead, H.G., McEuen, P.L., 2010. Large-scale arrays of single-layer graphene resonators. Nano Lett. 10, 4869–4873.
Zhu, R., Liu, X.N., Hu, G.K., Sun, C.T., Huang, G.L., 2014. A chiral elastic metamaterial beam for broadband vibration suppression. J. Sound Vib. 333, 2759–2773.

Please cite this article as: L. Lu, C.Q. Ru and X. Guo, Vibration isolation of few-layer graphene sheets, International Journal of Solids and Structures, https://doi.org/10.1016/j.ijsolstr.2019.08.029